J. Univ. Kuwait (Sci.) **14**, 1987

Line transients with corona

MOHAMED MOSTAFA SAIED, YOUSEF A. SAFAR AND MOHAMED H. SALAMA

Department of Electrical and Computer Engineering, University of Kuwait, P.O. Box 5969, Safat 13060, Kuwait

ABSTRACT

This paper investigates the effect of corona on the electromagnetic transients along high voltage overhead lines. A method is presented to simulate the line by dividing it into a number of sections connected in cascade. For n line sections, the number of the unknown variables is $2n + 1$. The method allows any waveform of the exciting voltage function, as well as any impedance loading condition. The corona is represented by voltage-dependent shunt current sources. A systematic way for writing a sufficient number of differential equations is shown. For their solution, a digital computer subroutine based on the Runge–Kutta–Verner method was used. An artificial frequency-dependent damping by means of linear resistors was used to suppress the Gibb's oscillations in the solution. The proposed method is applied to study the transients on a 40 km high voltage line with 30-ft flat phase spacing and a single 1·4 inch ACSR conductor per phase. The exciting voltage has a double-exponential impulse waveform. Solutions are given for three values of resistive loads Z_c, $2Z_c$ and $Z_c/2$, where Z_c is the line surge impedance. The results of two interesting cases of inductive and capacitive loads are also given. Physical interpretations for the different solutions are given. Also, the current-voltage duality between inductive and capacitive loads is recognized. The corona was found to attenuate and distort the travelling waves. For example, during one wave excursion, the reduction of the current wave peaks can reach values as high as 8·5%. The effect is more noticeable in the current than in the voltage waves. As expected, it increases also with the line corona losses. The effect of the increase of the line effective capacitance due to the corona discharge is also demonstrated.

INTRODUCTION

There are many available procedures which can be efficiently applied to get the necessary information about the transient behaviour of electric power networks and their different components. The results of these analyses are of great significance during the planning, design as well as the operation of such systems. They include, for example, the expected transient currents which can be one of the decisive factors in dimensioning some components such as bus bars, circuit breakers, machine windings, or in assessing the effectiveness of the protective schemes under some abnormal conditions, e.g. the influence of the transient inrush currents in power transformers.

Equally important, if not more so, are the power network voltage transients, which can be initiated by internal switching actions (specially important for extra high voltage networks), interference with proximate high voltage lines or by external atmospheric conditions. The latter are more significant in networks of relatively lower rated voltages. These overvoltages are important in coordinating the system insulation and the choice of types and locations of the surge arresters and circuit breakers. In the IEEE tutorial course, which gives a comprehensive review of the different techniques for the digital simulation of electrical transient phenomena (Phadke 1981), there is a list of 145 references, from which more than 40 are devoted only to transmission line transients using analog or digital simulation techniques. This gives an idea about the growing interest in that subject during the last two decades. One of the fundamental contributions is that made by Dommel (1969) about the digital computer solution of electromagnetic transients of single and polyphase networks leading to the development of the Electromagnetic Transients Program (EMTP) described by Meyer & Liu (1980) at the Bonneville Power Administration. Because the line parameters are generally frequency-dependent, many investigations have been made to take this into account when studying switching transients of overhead transmission lines (Semlyen & Kwok 1972).

One of the basic problems encountered when simulating power lines, however, is the presence of corona discharges. Because of the inherent nonlinearity of this phenomenon, the solution techniques have to be modified accordingly. Kudyan & Shih (1981) gave a *phenomenological* model to simulate the corona loss and the change of line capacitance. The model circuit for each line section includes a series inductance, three capacitors, two resistors and finally two ideal diodes, i.e. nine elements per section. The values of these equivalent elements could be found from the measured corona loss at the power frequency. The method was applied successfully to simulate the transients on three sample lines of critical corona voltages, 386, 589 and 685 kV, for a total line length of 2·5 km, each. Kudyan & Shih (1981) further stated that there is an upper limit on the line length, about 5 km, beyond which the computed solution appreciably deviates from the exact solution. This is because of the cumulative nature of the truncation error. Therefore, it becomes difficult to use this model in studying long lines. The method given by Harrington & Afghani (1983), based on a simpler shunt equivalent circuit, could be applied to study the switching transients on a 160 km long line. However, because a travelling wave approach has been applied, and in order to avoid possible wave reflections, the method could only be used to study lines with their surge impedance loadings. A remarkably simpler model for including the corona loss in the study of the power frequency overvoltages in series compensated EHV lines is given by Illiceto *et al.* (1984), where the corona is simulated by shunt nonlinear resistors determined from the static corona loss measurement. These resistors are assumed lumped in the intermediate point of the line. The justification for this was that the voltage drops on the line series impedances are very small. Although the method has been applied to relatively long lines of several hundreds of kilometers, the purpose of study was primarily to investigate the voltage at the line terminal points, so that no information is given about the voltage and current distributions along these lines.

It is the purpose of this paper to improve the accuracy of the method suggested (Illiceto *et al.* 1984) by increasing the number of the fictitious nonlinear resistors (or equivalent voltage-controlled current sources) and to distribute them more uniformly along the line. Moreover, it is intended to carry out the simulation in such a flexible

way, that also the current and voltage distributions along lines of any length can be obtained for any receiving-end loading condition and for different waveforms and amplitudes of the sending-end input voltage.

METHOD OF ANALYSIS

Consider the sample power transmission network shown in Fig. 1. It consists of a 3-phase high voltage transmission line supplying an impedance load connected at the receiving-end (RE). The equivalent circuit of the load comprises a parallel connection of three elements R_L, L_L and C_L. This is a flexible way of representation so that a load of any power factor can be easily modelled. It is assumed that at $t = 0$, an overvoltage transient $E(t)$ of internal or external type is initiated at a point P, at a distance L far from the receiving end. In the suggested method of analysis, there will be no restrictions on the voltage waveform of $E(t)$. It can have any analytical time expression, or can even be in a tabulated form. This overvoltage transient will result in a pair of travelling waves, one of which will propagate along the line towards the load. If the line is not terminated by its surge impedance, there will be reflections at RE causing wave propagation in the opposite direction. It is assumed that, in some locations, the voltage magnitudes along the line can exceed its critical corona onset voltage V_c, which can be easily determined from the line data, so that some portions of the line length will be subject to corona discharge. It is required to find the voltage and current distributions along the line, i.e. their values at any general point (at a distance x from point P), at any time t. To do that, the line has to be divided into n identical sections of the same length L/n. It is generally recommended that each section length should not exceed about 10 km (Greenwood 1971). Assuming R, L and C to be the values of the entire line series resistance, series inductance and shunt capacitance, respectively, then each section will have the values (R/n), (L/n) and (C/n), as shown in Fig. 2. The equivalent circuit

Fig. 1. Sample power network.

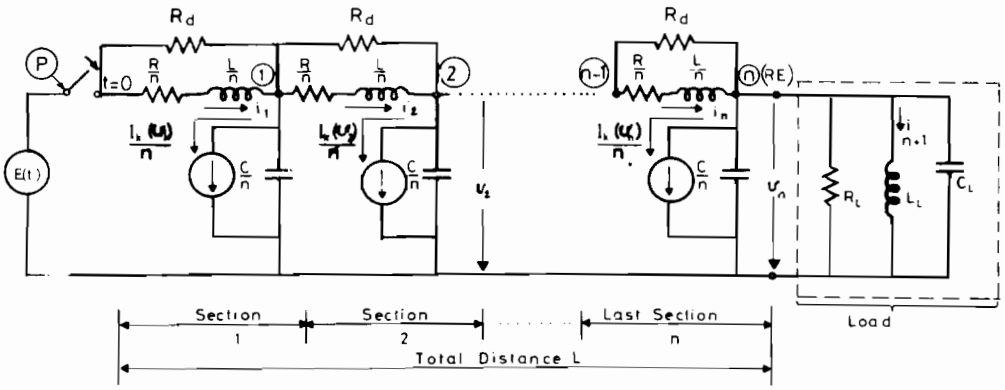

Fig. 2. Equivalent circuit for the line under corona.

includes also the load model, and n voltage-dependent current sources distributed equidistantly along the line to represent the corona currents. Their values will be zero, if the voltage at the corresponding node is less than or equal to V_c, otherwise it will depend on the instantaneous local value of the voltage v. The value $I_k(v)$ is assumed to be the total corona current, if the entire line distance L had the voltage v. The function $I_k(v)$ can be determined from the measured line corona loss curve as indicated in detail by Illiceto *et al.* (1984). It is shown that if a corona power loss measurement yields a value of p watts at a voltage of peak phase value V_m, then the slope of the linear part of the corona voltage–current characteristic ($R_k = dV/dI_k$) is given by

$$R_k = \frac{V_m}{\pi p}\left[V_m \cos^{-1}(z) - V_c\sqrt{1-z^2}\right] \tag{1}$$

where

$$z = \frac{V_c}{V_m}, \quad p \text{ is the corona loss}$$

and

V_c is the critical corona voltage (peak value to neutral).

In order to suppress the Gibb's oscillations expected in using the above inherently lumped parameter technique, the *damping* resistors R_d are connected in shunt with the line series elements, as shown in Fig. 2. This will yield a frequency-dependent damping effect. At low frequencies, the different R_d's will be shorted approximately by the relatively low series impedances of the line sections. For the higher frequencies of the Gibb's oscillations, most of the longitudinal currents will flow through the damping resistors. Using the line longitudinal currents $i_1, i_2, \ldots, i_m, \ldots, i_n$ and the voltages $v_1, v_2, \ldots, v_n$, as well as the current through the load inductance i_{n+1} as the network time variables, the following differential equations can be easily derived:

a) Current derivatives:

$$\begin{aligned}
i_1' &= \frac{n}{L}\left[E(t) - v_1 - i_1\left(\frac{R}{n}\right)\right] \\
i_2' &= \frac{n}{L}\left[v_1 - v_2 - i_2\left(\frac{R}{n}\right)\right] \\
&\vdots \\
i_m' &= \frac{n}{L}\left[v_{m-1} - v_m - i_m\left(\frac{R}{n}\right)\right] \\
&\vdots \\
i_n' &= \frac{n}{L}\left[v_{n-1} - v_n - i_n\left(\frac{R}{n}\right)\right] \\
i_{n+1}' &= v_n/L_L.
\end{aligned} \tag{2}$$

b) Voltage derivatives:

$$\begin{aligned}
v_1' &= \frac{n}{C}\left[i_1 - i_2 - I_k(v_1)/n + \{E(t) - 2v_1 + v_2\}/R_d\right] \\
&\vdots \\
v_m' &= \frac{n}{C}\left[i_m - i_{m+1} - I_k(v_m)/n + \{v_{m-1} - 2v_m + v_{m+1}\}/R_d\right] \\
&\vdots \\
v_n' &= \left[i_n - I_k(v_n)/n - v_n/R_L - i_{n+1} - \{v_n - v_{n-1}\}/R_d\right]/(C_L + C/n).
\end{aligned} \tag{3}$$

There will be $n + 1$ current derivative and n voltage derivative equations. The total number of equations (or unknowns) is $2n + 1$. Their solution gives the required current and voltage distributions. Any of the known numerical solution techniques can be used to get the time dependence of each of these $2n + 1$ unknowns. In this study, a subroutine based on the Runge–Kutta–Verner fifth- and sixth-order method for the solution of a system of first-order ordinary differential equations of the form $y' = f(x, y)$ with initial conditions was used. It provides several options including different kinds of error control and restrictions on step sizes. It also attempts to keep the global error proportional to a tolerance specified by the user.

APPLICATION AND RESULTS

The above described method was used to study the effect of corona on the voltage and current distributions during some energization transient conditions of an overhead 3-phase transmission line having the following data (Weeks 1981):

Line length	40 km
Conductors per phase	1
Conductor type	1·4 inch, ACSR
Configuration	30-ft flat spacing.

From these values, the following constants can be easily derived:

Resistance	0·045 Ω/km
Inductance	$1{\cdot}346 \times 10^{-6}$ H/m
Capacitance	$8{\cdot}55 \times 10^{-12}$ F/m.

Critical corona voltage at standard temperature and pressure $V_c = 116$ kV (RMS) to neutral, which is also available from test results in Weeks (1981).

The time taken by the electromagnetic waves to travel along the line can be estimated to be 40 km/velocity of light, i.e. 3×10^5 km/sec = 133 μsec. The number of line sections was taken $n = 64$ (i.e. 625 m/section). Because the corona loss depends largely on the atmospheric conditions as well as the conductor surface roughness, three different values for the corona loss p were assumed at a certain test value of the line voltage (400 kV), i.e. $V_m = 400\sqrt{2}/\sqrt{3}$ kV to neutral:

case A $p = 0$ (which means simulation without corona)
case B $p = 20$ W/m
case C $p = 100$ W/m (extreme conditions).

In this particular case study, a value of the damping resistance $R_d = 1$ kΩ per section was found to be most suitable for suppressing the Gibb's oscillations in the voltage and current signals. Several program runs have been made for different magnitudes and waveforms of the exciting voltage $E(t)$. Also, different receiving-end terminations have been considered, such as proper termination by the line surge impedance ($Z_c = 400$ Ω), pure resistance termination with half and double this value for the load resistance, open- and short-circuited receiving end, pure inductive and pure capacitive loadings. For each of these case studies, the UNIVAC 1100 computer at Kuwait University required on the average 40·5 sec CPU time. For example, Figs 3a–c give the distributions of the voltage, current and corona current, respectively, for a double-exponential input voltage $E(t)$. The load impedance is assumed pure resistive

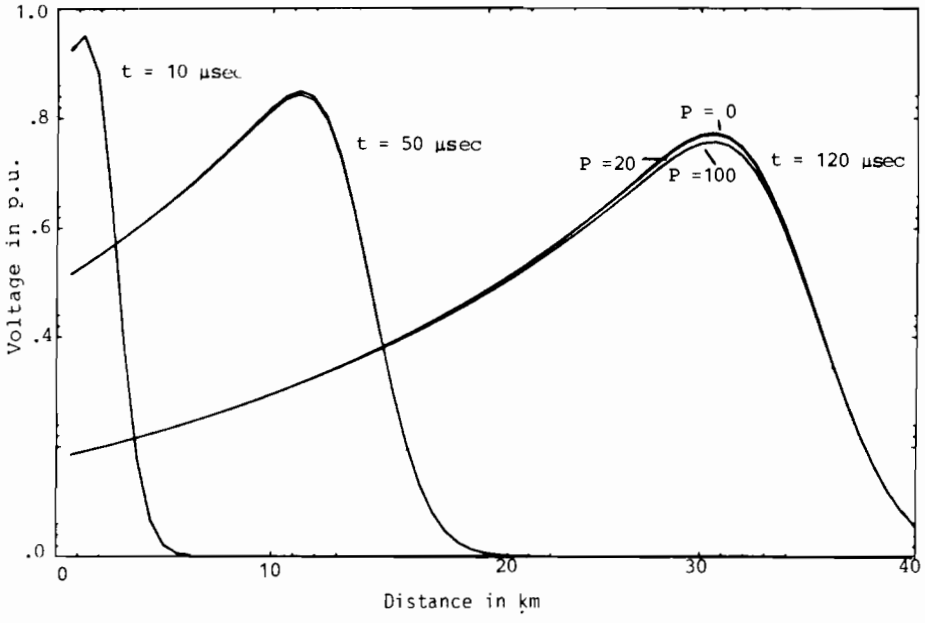

(a)

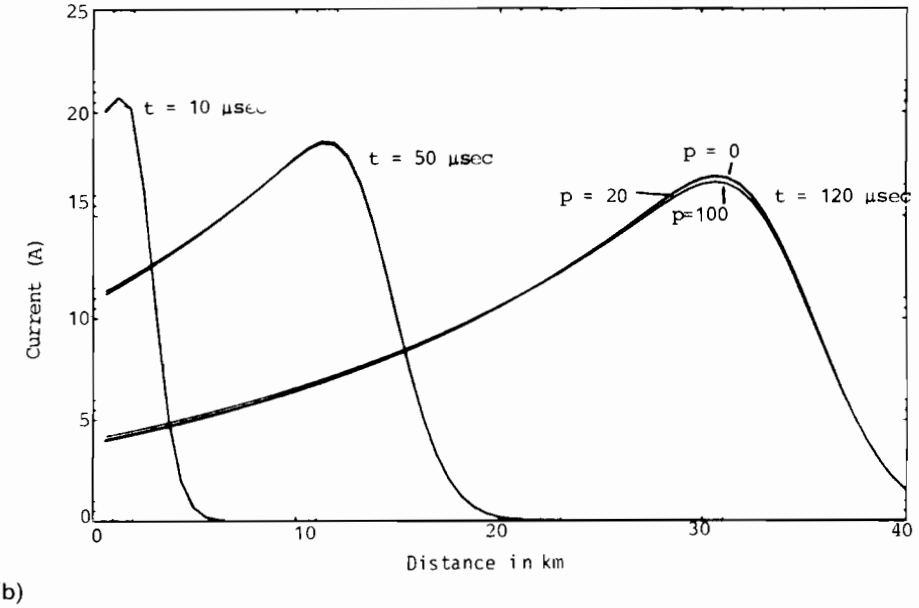

(b)

Fig. 3. Electromagnetic transients following a double-exponential input. The line is properly terminated by $R_L = Z_c$.
(a) Voltage distribution.
(b) Current distribution.

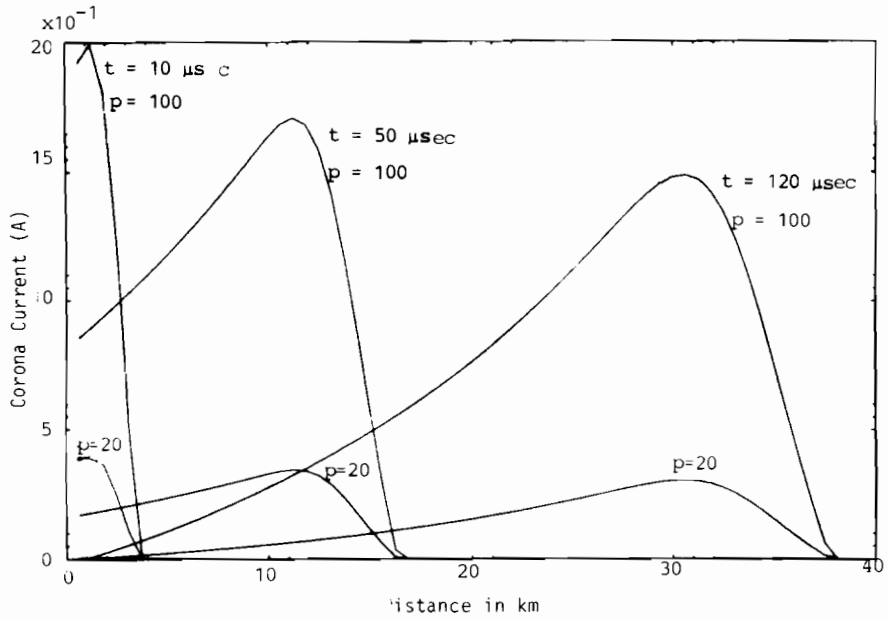

(c)

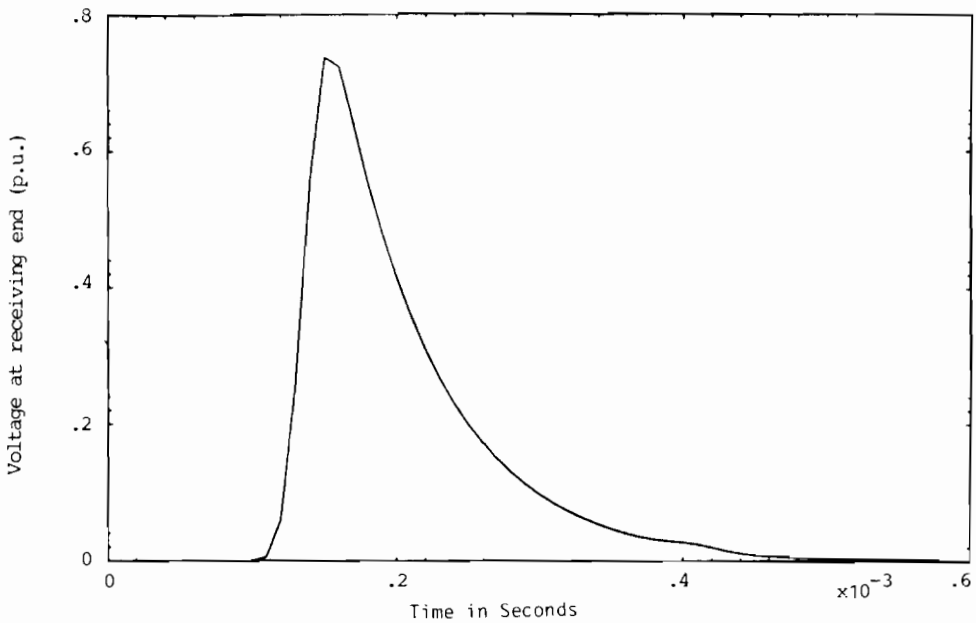

(d)

(c) Corona current distribution.
(d) Receiving-end voltage.

$R_L = Z_c = \sqrt{L/C} = 400\ \Omega$. This can be represented by putting $L_L = \infty$ and $C_L = 0$ in the equivalent circuit in Fig. 2. The solutions are given for the time points 10, 50 and 120 μsec. The voltage $E(t)$ is given by

$$E(t) = 900[\exp(-t/68{\cdot}5) - \exp(-t/0{\cdot}405)]\ \text{kV} \tag{4}$$

where t is the time in μsec, which represents a 828 kV impulse voltage for which the front and tail times can be easily found (Kind 1972). The voltage scale is given in per unit based on the surge peak value of 828 kV. From the three figures, the wave nature of the signals as well as the damping effect of the corona can be easily recognized. During propagation, the peaks of the voltage and current waveforms are gradually attenuated and distorted. This effect increases for higher values of the corona loss p. For comparison, the distributions are also given for zero corona loss ($p = 0$). Comparing Figs 3a and 3b, it can be seen that for each case study, the voltage and current distributions are almost proportional (ratio v/i corresponds to the line surge impedance $Z_c = \sqrt{L/C} = 400\ \Omega$). Also, the attenuation due to corona is more clear in the current than in the voltage distributions. Detailed information about the corona current distributions are depicted in Fig. 3c. For all cases denoted by $p = 0$, the corona currents are obviously zero. For the extreme case $p = 100$, these shunt currents can attain values as high as 2 A/section (i.e. 3·2 A/km), whereas for cases $p = 20$, it reaches about 0·4 A/section (or 0·64 A/km). By investigating the solutions for time points after the arrival of the travelling waves at the receiving end, it was noticed that no reflections occur when the line was terminated (pure resistively) by its surge impedance of 400 Ω, as expected. This is more clear from Fig. 3d giving the time function of the voltage at the load terminals for the three cases $p = 0$, 20 and 100 W/m. It can also be noticed that the receiving-end voltage remains practically zero until the propagation time of one excursion (i.e. 40 km/3 $\times$ 10^5 km/sec $\approx$ 133·3 μsec) elapses.

Fig. 4 shows the distributions for the same impulse voltage $E(t)$, but the line is now terminated by a pure resistive load of double the value of the surge impedance (i.e. $R_L = 800\ \Omega$). This will enable us to study the reflections at the receiving end, RE. Fig. 4a for the voltage depicts clearly the voltage increase at RE at 150 μsec (shortly after the arrival of the incident wave) which is due to the positive voltage reflected wave. The damping effect of corona is negligible at points having instantaneous values of the voltage less than 165 kV (the peak critical voltage). The current curves shown in Fig. 4b show the effect of the (negative) current reflected wave at $t = 150$ μsec. Comparing the curves for the three successive points, it can be seen that the current at the receiving end is decaying gradually after the arrival of the incident wave peak value. From Fig. 4c giving the corona currents, it is observed that this current is always positive for all points along the line, because the corresponding voltages in Fig. 4a are also positive. It can also be noticed that, just after the first reflection at RE, the corona current can attain values of about 2 A/section (3·20 A/km), at the time points 150 μsec and 250 μsec. The corona current in the first 8 km near the sending end, SE, is zero, because the corresponding voltages are seen in Fig. 4a to be less than the peak critical voltage 165 kV. The voltage at RE is depicted in Fig. 4d as a function of time for $p = 0$ and $p = 100$ W/m. Also here the time delay of 133·3 μsec with respect to the SE voltage signal can be clearly recognized. The effect of the wave reflections is noticeable at $t \approx 400$ μsec, where the second incident wave of negative polarity (due to the assumed source internal resistance) arrives at the receiving end, RE.

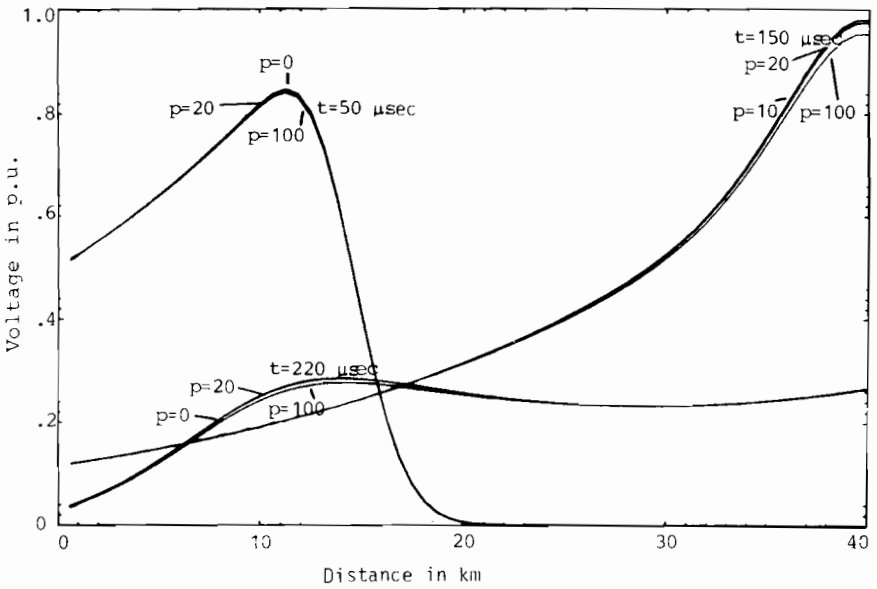

(a)

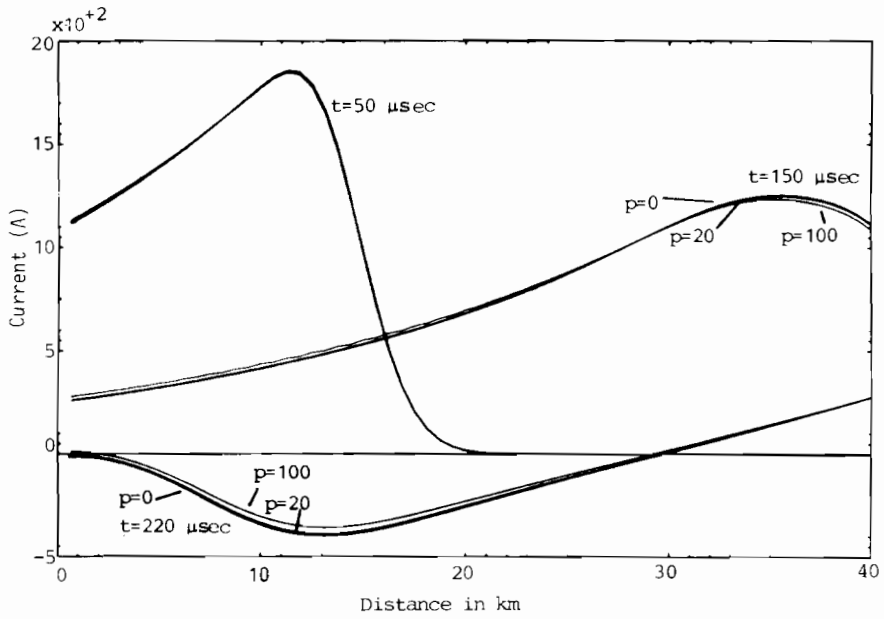

(b)

Fig. 4. Electromagnetic transients following a double-exponential input. The line is properly terminated by $R_L = 2Z_c$.
(a) Voltage distribution.
(b) Current distribution.

(*Fig. 4 continued overleaf*)

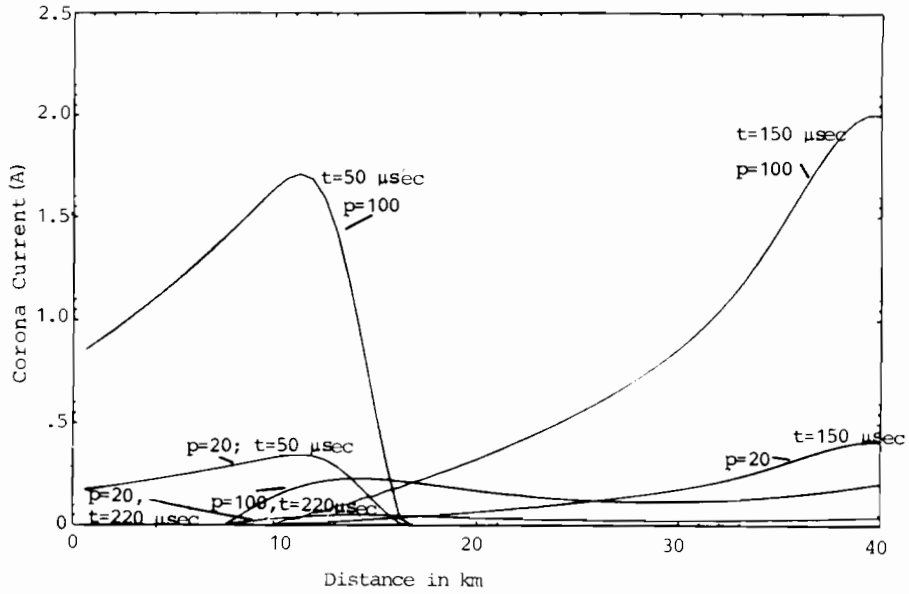

(c)

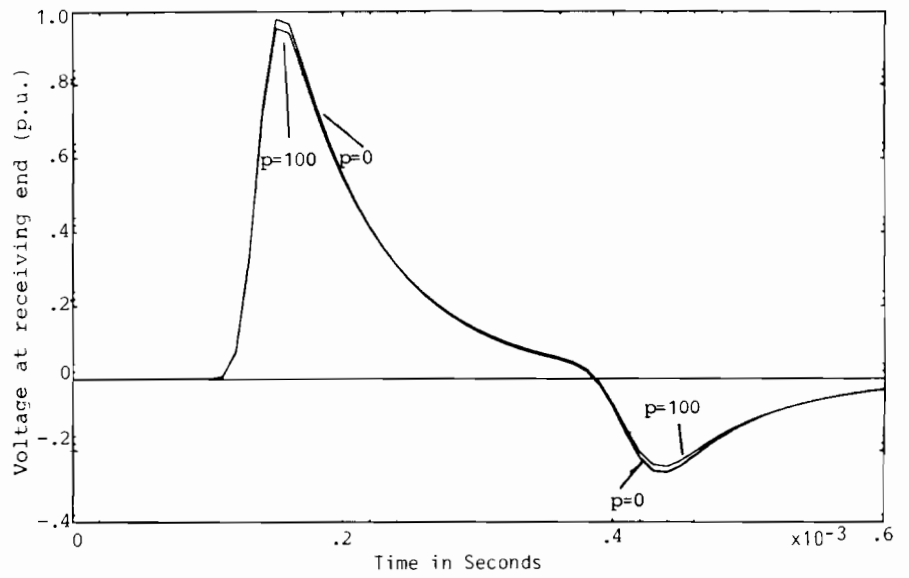

(d)

(c) Corona current distribution.
(d) Receiving-end voltage.

The results for a line termination by half the line surge impedance (200 Ω), which are not given here due to space limitations, showed a current distribution which is similar and almost proportional to the voltage distribution in the case of termination by $2Z_c$ (800 Ω), and vice versa. This is explained by the fact that for these two terminations, the reflection factors at the receiving end are equal in magnitude, but opposite in sign.

The effect of the load power factor is best illustrated by the following case study, with the results given in Fig. 5. Here, the load impedance is assumed pure inductive ($\cos\phi = 0$ lagging). The magnitude of the reactance at the rated frequency 50 Hz is equal to the surge impedance (400 Ω). This can be simulated by putting $R_L = \infty, C_L = 0$ (see Fig. 2). The input voltage has the same waveform as in the previous cases. The voltages are shown in Fig. 5a. At $t = 50\,\mu$sec, the incident waves propagated about 15 km from the sending end. Curves are also given for the conditions after 150 μsec, i.e. shortly after the arrival of the incident wave. The voltage is seen to have the value of about 1·5 MV at the receiving end. This is because the inductor acts during the reflection of the wave front approximately as an open circuit, giving a reflection factor of about unity. At these high values of voltage, the effect of the corona losses is considerable. This can also be seen in Fig. 5b giving the current distributions, where at the time point 250 μsec, the difference between the current curves for $p = 0$ and $p = 100$ W/m reaches about 8·5%. The damping can also be estimated by comparing the peak currents at 50 μsec (about 1·9 kA) and at 250 μsec (about 1·4 kA). The curves on Fig. 5c give the corona current distributions. Interesting are the relatively large corona currents near the receiving end, shortly after the first wave reflection. Due to the excessive voltage values (see Fig. 5a) the corona current can reach values as high as 3·2 A/section (5·1 A/km). Notice also the relatively small corona currents near the receiving end at 250 μsec. The receiving-end voltage is shown in Fig. 5d. The effect of the first reflection is noted at $t \approx 133\,\mu$sec, where the voltage attains an excessive peak value due to the positive reflection coefficient. This explains also the negative peak at $t \approx 400\,\mu$sec (i.e. three wave excursions along the line).

For comparison, Fig. 6 gives the voltages and currents for the same input signal $E(t)$, but with the line terminated by a purely capacitive load. The capacitive reactance at 50 Hz was assumed to be equal to Z_c (400 Ω). This can be simulated by putting the load resistance $R_L = \infty$ and load inductance $L_L = \infty$ in Fig. 2. The similarity between the voltage distributions in this case (Fig. 6a) with the current distributions in the previous one (Fig. 5b) as well as the similarity of Fig. 6b for the currents to Fig. 5a for the corresponding voltages, show clearly the duality between the two cases of pure inductive and pure capacitive termination (Kind 1972). During the reflection process at the receiving end, the load capacitor acts momentarily as a short circuit. This is the reason for the relatively low voltage values at the receiving end in Fig. 6a, and the corresponding relatively high line currents (about 3·2 kA) in Fig. 6b. The load voltage is depicted in Fig. 6d, where the negative reflection coefficient due to the very small load reactance during the first reflection at $t \approx 133\,\mu$sec can be noticed. Also, the positive second incident wave resulting from the negative reflection coefficients at the source side shows itself clearly at $t \approx 400\,\mu$sec. Fig. 7 gives the time waveform of the voltage at the open-circuited receiving end, following a 50 Hz sending end energizing voltage of the cosine function

$$E(t) = 900\cos(314t)\,\text{kV}. \tag{5}$$

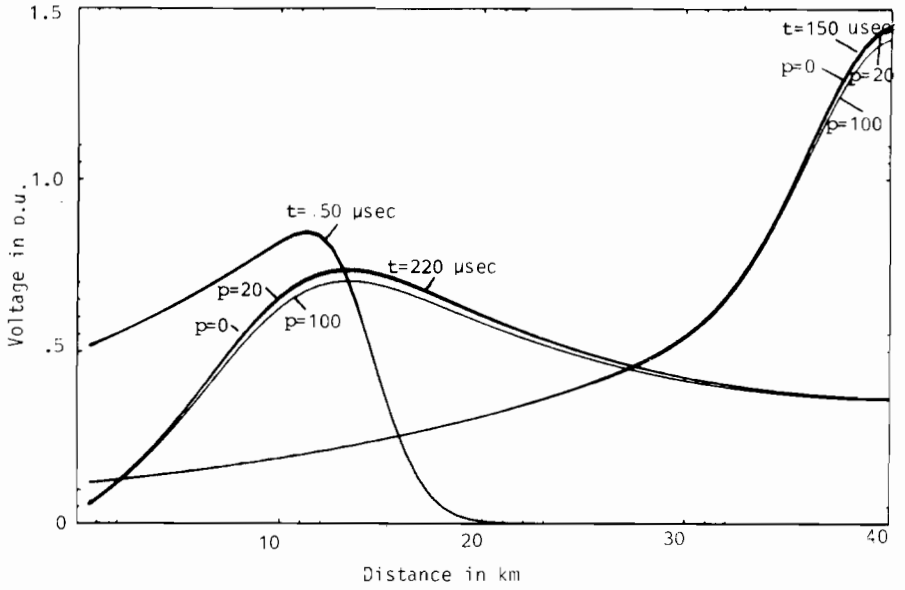

(a)

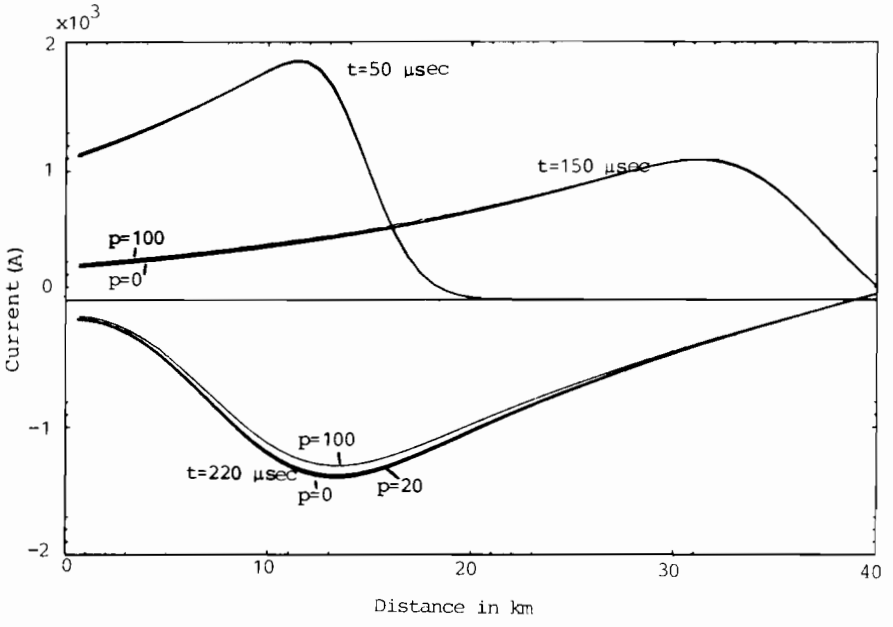

(b)

Fig. 5. Electromagnetic transients following a double-exponential input. The line is properly terminated by a purely inductive reactance $X_L = jZ_c$.
(a) Voltage distribution.
(b) Current distribution.

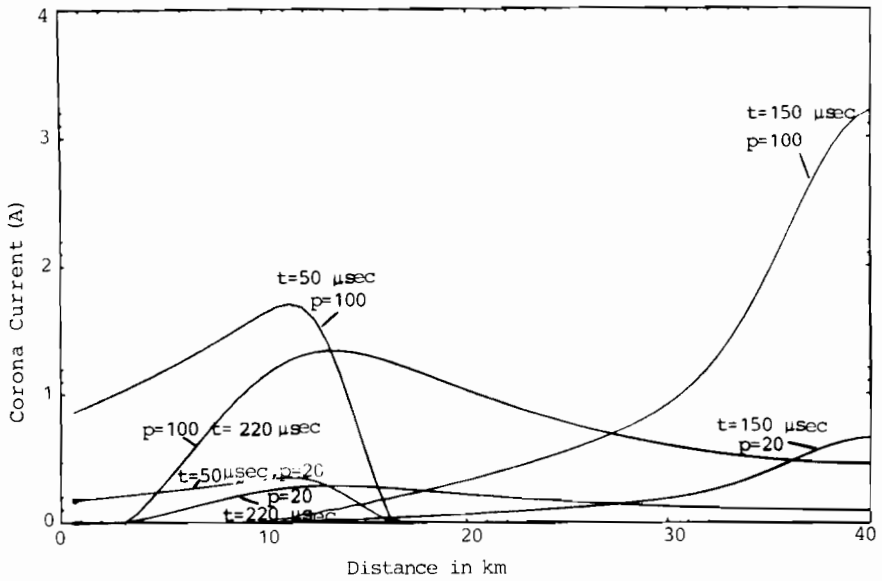

(c)

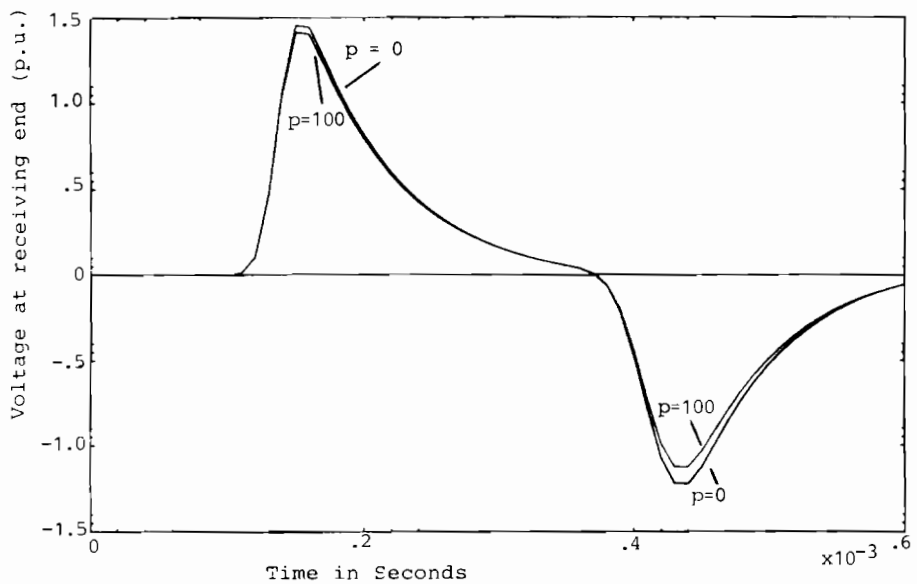

(d)

(c) Corona current distribution.
(d) Receiving-end voltage.

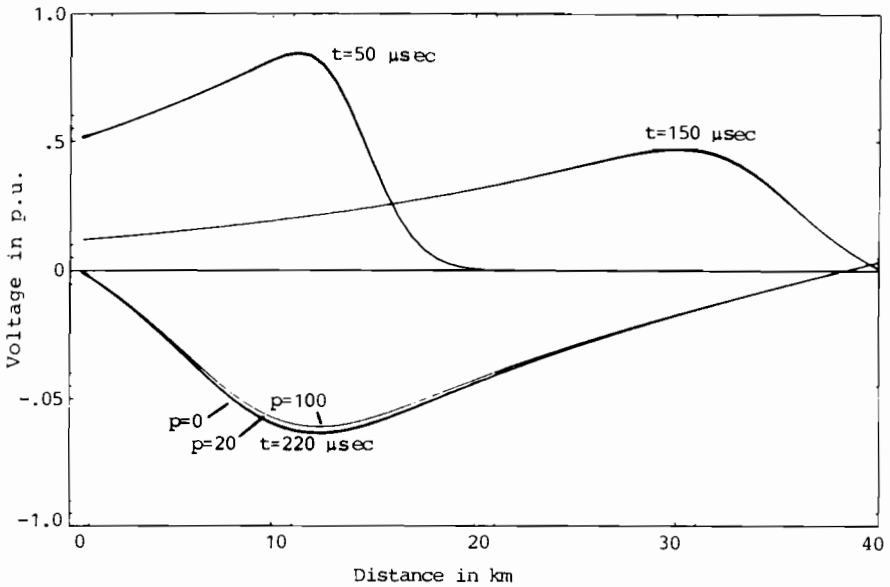

(a)

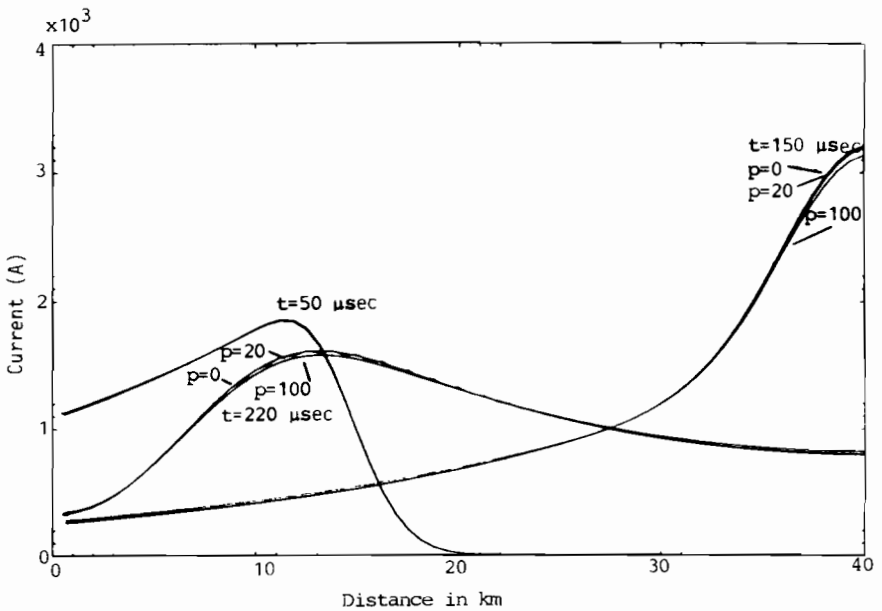

(b)

Fig. 6. Electromagnetic transients following a double-exponential input. The line is properly terminated by a purely capacitive reactance $X_c = -jZ_c$.
(a) Voltage distribution.
(b) Current distribution.

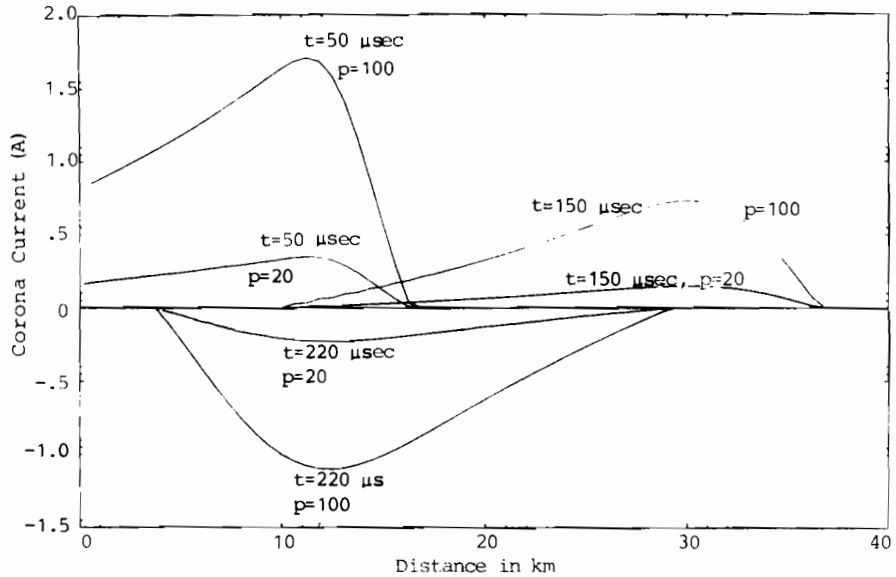

(c)

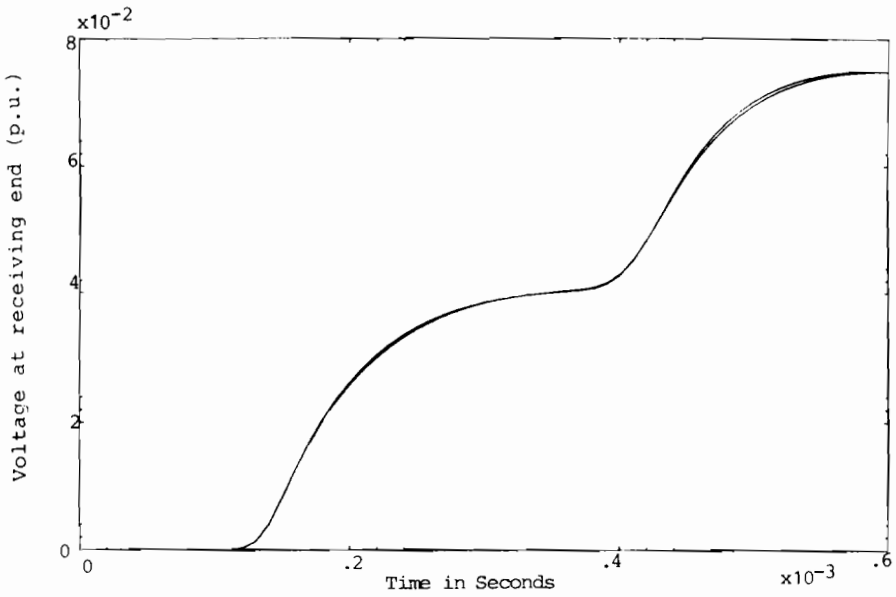

(d)

(c) Corona current distribution.
(d) Receiving-end voltage.

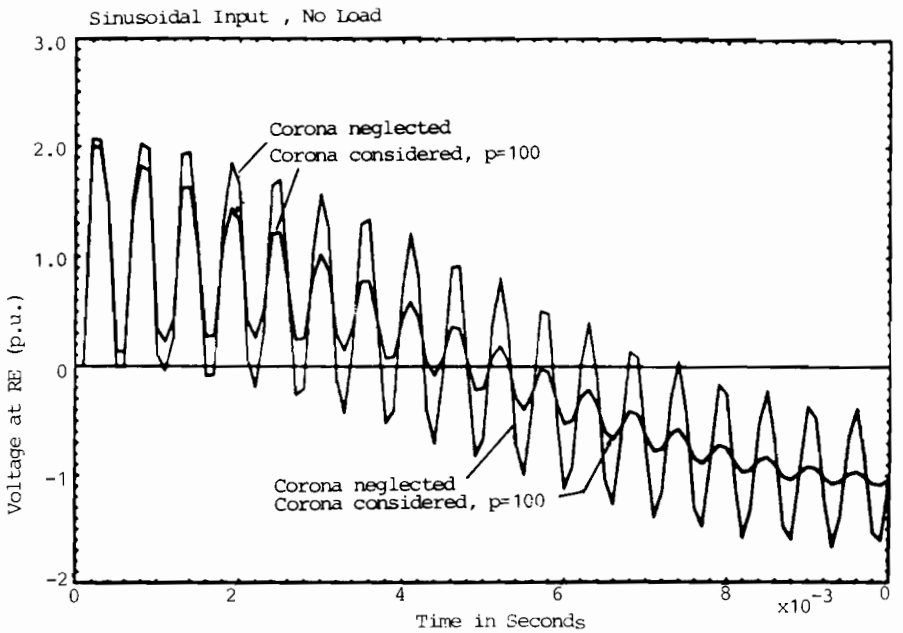

Fig. 7. Waveform of the voltage at the open-circuited receiving end due to a 50-Hz sending-end voltage: $E(t) = 900\cos(314t)$ kV.
(a) Corona neglected.
(b) Corona considered.

The instantaneous voltage values are shown in per unit based on the peak value 900 kV. Two cases are demonstrated. The first curve was calculated neglecting the effect of the line corona. This curve agrees quite well with the results found in the literature for this case (Marti 1982). Because of the unity reflection factor at the receiving end, its voltage can momentarily reach 2 pu. The different reflections at the line receiving end are clearly recognized, indicating the excursion time of 133 μsec, resulting in superimposed higher frequency almost sustained oscillations of about 1875 Hz. In the second curve, the corona discharge is considered, with $p = 100$. Although the frequency (1875 Hz) of these additional high frequency signals remains practically unaffected by the corona discharge, these components are seen to decay gradually, approaching the curve of the sinusoidal supply voltage.

The following case study is given to show the effect of the increased line *effective* capacitance due to corona. Actually, the coronized lines show a charge-voltage characteristic having the form of a hysteresis loop (Ovick & Kusic 1984; Inoue 1985), rather than a linear characteristic having a slope given by the line *intrinsic* capacitance, if this effect was neglected. There are many ways to take this local-voltage-dependent increase of the conductor *effective* radius into account. The approach presented by Ovick & Kusic (1984) has been adopted. It is based on the following relationship between the effective radius at a certain point along the line, and the relevant local instantaneous voltage

$$v = E_{\text{ion}}(r_c - r_w) + E_{\text{ion}} \cdot r_c \cdot \ln\left(\frac{h}{r_c}\right) \tag{6}$$

where

v local voltage value, v
E_{ion} air electric field strength, v/m
r_c local effective conductor radius, m
r_w actual conductor radius, m (1·778 cm in this example)
h conductor height above ground, m (30 m in this example).

The radii at the n line sections are generally different, and can be iteratively determined using the following modified form of Equation (6), written for the line section number m, e.g.

$$r_{c(m)} = (v_m + r_w \cdot E_{ion})/[E_{ion} \cdot \ln\{H \cdot e/r_{c(m)}\}] \tag{7}$$

where $e = 2{\cdot}718\,281\,28$. The resulting radius can be substituted in the right-hand side of Equation (7) to get a better estimate for r_c, and so on.

The results depicted in Fig. 8 give the receiving-end voltage in per unit based on 900 kV due to a 50 Hz switching voltage of peak value 900 kV at the sending end of the cosine form given by Equation (5), using four line sections and allowing for 10 iterations according to Equation (7), for every line section. Three curves are given in Fig. 8:

(a) with neglecting corona, i.e. putting $p = 0$, $r_c = r_w$;

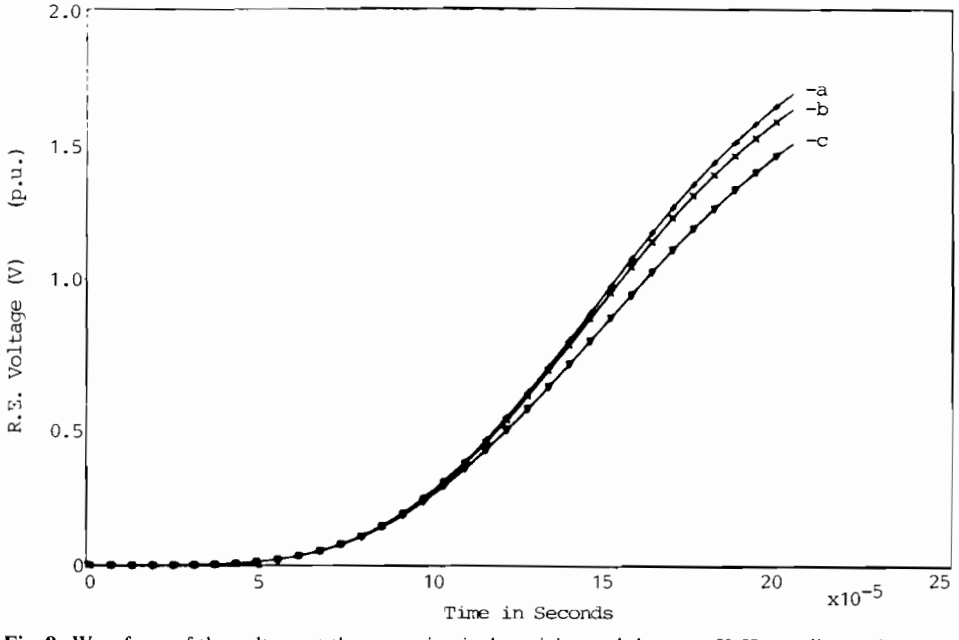

Fig. 8. Waveform of the voltage at the open-circuited receiving end due to a 50-Hz sending-end voltage: $E(t) = 900\cos(314t)$ kV.
(a) Neglecting corona.
(b) Corona considered, with constant radii.
(c) Corona considered, with variable radii and effective line shunt capacitance.

(b) with considering corona (with $p = 100$) but assuming that the conductor effective radii remain unchanged $= r_w$;
(c) with the corona considered (with $p = 100$) and taking the changes in the located radii into account.

From the previous considerations, if the line was lossless and corona neglected, the peak value would reach 2 pu (i.e. 1800 kV), due to the open-circuited receiving end.

The difference between curves (a) and (b) in Fig. 8 is due to the corona loss simulating voltage-dependent shunt current sources shown in Fig. 2, whereas the reduction from curve (b) to curve (c) is due to the consideration of the voltage-dependent changes in the local effective conductor radii simulating the corona discharge around the line conductor.

CONCLUSIONS

1. A method is presented to study the electromagnetic transients on high voltage overhead lines, taking into account eventually existing corona discharges. The analyses are based on the time domain numerical solution of a set of nonlinear differential equations. The corona is represented by distributed voltage-dependent current sources. Longitudinal shunt damping resistors were used to yield frequency-dependent damping and hence suppress the Gibb's oscillations. The solution gives the voltage, line longitudinal currents as well as the corona shunt current as functions of the location and the time.
2. The procedure was used effectively to study several cases of the line terminations starting from matched loading and improper termination by resistive load to pure inductive and capacitive loads. There is no limitation on the time waveform of the exciting voltage stimulus, although only results for double-exponential and power-frequency switching input voltage are given. The current–voltage duality between purely inductive and purely capacitive loads was recognized, and physical interpretations for the different solutions are given.
3. The corona was found to attenuate and distort the travelling waves. For example, during one excursion the reduction of the current wave peaks can reach values as high as 8·5%. The effect is more noticeable in the current than in the voltage waves. As expected, it increases also with the line corona losses, i.e. under foul weathering conditions and/or excessively rough conductor surfaces.
4. A case study was investigated to show the contributions of both the voltage-dependent shunt current sources simulating the corona power loss and the voltage-dependent charges in the local effective line capacitances, on the distortion and attenuation of the line electromagnetic transients, due to corona.
5. Investigations are now running in order to allow more detailed modelling of the line. They are based on 3-phase analysis including the effect of asymmetrical tower configuration, with and without transposition. Also, eventually existing line series or shunt compensating elements, as well as the different types of lightning arrestors and nonlinear inductors will be considered.
6. It is believed that the suggested method enables the engineer to get useful information for the design, analysis and operation of high-voltage lines.

ACKNOWLEDGEMENT

This work was supported by Research Grant No. EE 011, Kuwait University. Also, partial support was provided by Research Grant No. EE 028, Kuwait University.

REFERENCES

Dommel, H.W. 1969. Digital computer solution of electromagnetic transients in single and multiphase networks. IEEE Transactions on Power Apparatus and Systems **88**: 388–99.

Greenwood, A. 1971. Electrical transients in power systems. Wiley Interscience.

Harrington, R.J. & Afghani, M. 1983. Implementation of a computer model to include the effects of corona in transient overvoltage calculations. IEEE Transactions on Power Apparatus and Systems **102**(4): 902–10.

Illiceto, F., Cinieri, C. & Di Via, A. 1984. Overvoltages due to open-phase occurrence in reactor-compensated EHV lines. IEEE Transactions on Power Apparatus and Systems **103**(3): 474–82.

Inoue, A. 1985. Propagation analysis of overvoltage surges with corona based upon charge versus voltage curve. IEEE Transactions on Power Apparatus and Systems **104**(3): 655–62.

Kind, D. 1972. Einführung in die Hochspannungsversuchstechnik. Vieweg Verlag, Braunschweig (West Germany).

Kudyan, H.M. & Shih, C.H. 1981. A nonlinear circuit model for transmission lines in corona. IEEE Transactions on Power Apparatus and Systems **100**(3): 1420–30.

Marti, J.R. 1982. Accurate modelling of frequency-dependent transmission lines in electromagnetic transient simulations. IEEE Transactions on Power Apparatus and Systems **101**(1): 147–55.

Meyer, W.S. & Liu, T.H. (Eds). 1980. Electromagnetic transients program (EMTP) rule book. Bonneville Power Administration, Portland, Oregon, 750 pp.

Ovick, N.L. & Kusic, G.L. 1984. Including corona effects for travelling waves on transmission lines. IEEE Transactions on Power Apparatus and Systems **103**(12): 3643–9.

Phadke, A.G. 1981. Digital simulation of electrical transient phenomena. IEEE Tutorial Course, Publication 81EH0173-5-PWR.

Semlyen, A. & Kwok, M.C. 1972. Calculation of switching transients on overhead transmission lines with frequency-dependent elements, part I—Theory. IEEE Paper No. C72-563-5 presented at the Power Engineering Society Summer Meeting, San Francisco.

Weeks, W.L. 1981. Transmission and distribution of electrical energy. Harper & Row, New York.

(Received 16 March 1985, revised 17 May 1986)

التغيرات الكهرومغناطيسية اللحظية على خطوط الجهد العالي في وجود الكورونا

محمد مصطفى سعيد يوسف عبدالنبي صفر محمد حسن سلامة
قسم الهندسة الكهربائية والكمبيوتر بجامعة الكويت ، ص . ب ٥٩٦٩ ، الصفاة ١٣٠٦٠ ، الكويت

خلاصة

تبحث هذه الدراسة في تأثير ظاهرة التوهج الكهربي (الكورونا) على التغيرات اللحظية في كل من الجهد والتيار الكهربي لخطوط الجهد الفائق المستخدمة في نقل الطاقة الكهربائية . وتعتمد هذه الدراسة على وضع نموذج لخط النقل بعد تقسيمه الى عدد كاف من الأجزاء المتماثلة والمتصلة على التتابع . وتسمح طريقة المعالجة الرياضية لخط النقل بعد تمثيله رياضيا بدراسة تأثير الأشكال المختلفة لموجة الجهد عند أي نوع من أشكال التحميل لخط نقل القوى . وباستخدام برنامج للحاسب الآلي يعتمد على طريقة رنج ـ كوته ـ ڤيرنر الخاصة بالتحليل العددي للمعادلات التفاضلية فلقد تم الحصول على نتائج من مجموعة المعادلات التفاضلية الناتجة عن تمثيل خط النقل . ولأخماد الذبذبات الناتجة من هذا الحل الرياضي للمعادلات فلقد تمت الأستعانة بمقاومات خطية في الدائرة المكافئة .

ولقد استخدمت هذه الطريقة الرياضية لدراسة التغيرات اللحظية على خط هوائي يعمل عند جهد *220* كيلو فولتا بطول *40* كيلو مترا ويتكون من ثلاثة أوجه يبعد كل منها عن الآخر مسافة مستقيمة قدرها *30* قدما ويشتمل كل وجه على موصل واحد قطره *1,4* بوصة . وأوضحت نتائج برنامج الحاسب أن تعرض شبكة ما لظاهرة التوهج الكهربي سوف يعمل على تخميد وتشويه الموجات الكهربية المتنقلة ، وفي بعض الحالات قد تصل نسبة تخميد موجة التيار الى معدل *8½%* ، ويزداد هذا الأضمحلال مع زيادة مفقودات التوهج الكهربي . وتتضح ظاهرة الأضمحلال هذه في موجات التيار أكثر مما تتضح في موجات الجهد ، كما أوضحت النتائج أن السعة المؤثرة للخط تزداد عند تواجد ظاهرة التوهج الكهربي .